Rapid Communications

Antiferromagnetic order survives in the higher-order quasicrystal approximant

S. Yoshida,[1] S. Suzuki,[1] T. Yamada,[2] T. Fujii,[3] A. Ishikawa,[1] and R. Tamura[1,*]

[1]*Department of Materials Science and Technology, Tokyo University of Science, Niijuku, Tokyo 125-8585, Japan*

[2]*Department of Applied Physics, Tokyo University of Science, Niijuku, Tokyo 125-8585, Japan*

[3]*Cryogenic Research Center, The University of Tokyo, Bunkyo, Tokyo 113-0032, Japan*

(Received 4 September 2019; published 25 November 2019)

We report the observation of antiferromagnetic (AFM) transitions in 1/1 and 2/1 quasicrystal approximants having slightly different electron-per-atom (e/a) ratios, in the same Au-Ga-Eu system, at Néel temperatures of 7.0 and 8.5 K, respectively. This clearly demonstrates that an antiferromagnetic order survives when the degree of approximation to the quasicrystals is raised provided that the e/a ratio is kept nearly the same. Since, unlike the 1/1 approximant, the 2/1 approximant has all the building blocks necessary for the construction of the quasicrystal, this finding can be a significant leap toward the long-sought realization of an AFM quasicrystal.

DOI: 10.1103/PhysRevB.100.180409

Soon after the discovery of the binary icosahedral quasicrystal $Cd_{5.7}Yb$ in 2000 [1,2], its crystalline analogs, the so-called Tsai-type 1/1 and 2/1 cubic approximants, were identified in Cd_6Yb and $Cd_{76}Yb_{13}$, respectively [3,4]. Since then, the Tsai-type approximants have been the target of growing interest because a number of novel phenomena have been reported in the last two decades, including unique low-temperature order-disorder transitions [5–9], rich magnetic transitions [10–20], valence fluctuations [21,22], quantum critical phenomena [23], and superconducting transitions [24–26].

The Tsai-type 1/1 and 2/1 cubic approximants can both be described as a packing of rhombic triacontahedron (RTH) clusters. The RTH cluster consists of four concentric shells, from the center outwards: a tetrahedron of 4 atoms, a dodecahedron of 20 atoms, an icosahedron of 12 rare-earth (R) atoms, an icosidodecahedron of 30 atoms, and an RTH of 92 atoms [3,27], as depicted in Fig. 1(a). The atomic structure of the 1/1 approximant is a bcc packing of RTH clusters, while the 2/1 approximant has a different packing manner: An additional unit called an acute rhombohedron (AR) is necessary for the construction of the 2/1 approximant [27]. In the 2/1 approximant, the ARs fill the gaps between the RTH cluster network and each AR has two R atoms located on its longer body diagonal, as shown in Fig. 1(b). Figures 1(c) and 1(d) show the atomic arrangements of R atoms in the 1/1 and 2/1 approximants, respectively. In both structures, the RTH cluster network consists of two types of linkages, viz., b and c linkages, as shown in Figs. 1(e) and 1(f), respectively. In the b linkage, the clusters touch each other, sharing a rhombic face, while in the c linkage, the clusters interpenetrate sharing an obtuse rhombohedron [27,28].

One of the main structural differences between the 1/1 and 2/1 approximants is that the 2/1 approximant contains ARs, which are necessary for the construction of the quasicrystal structure, whereas the 1/1 approximant does not [3,27,28]. Thus, in order to clarify the condition of the antiferromagnetic (AFM) order in quasicrystal-derived materials more generally, it is important to determine whether the AFM order in the 1/1 approximant persists in higher-order approximants such as the 2/1 approximant, provided the key controlling parameter for the magnetism, i.e., the electron-per-atom (e/a) ratio, is kept nearly constant.

Since the discovery of quasicrystals in 1984 [29], no AFM quasicrystal has been reported to date and an AFM order was reported only in the binary 1/1 Cd_6R [10,13,14] until the recent observation of the first ternary AFM 1/1 approximants Au-Al-(Gd,Tb) in 2018 [20]. This finding of the ternary AFM approximants has opened up a different route to synthesize a number of other ternary AFM approximants by simply tuning the e/a ratio, i.e., replacing the Cd in Cd_6R by two other elements. Thus, we employ this approach for the search and synthesis of different AFM approximants in this Rapid Communication, and report here AFM transitions in both the 1/1 and 2/1 AFM approximants in the *same* alloy system, which clearly verifies that the AFM order survives in the higher-order approximant that has all the building blocks of the quasicrystal.

Polycrystalline alloys having two slightly different compositions, $Au_{66}Ga_{20}Eu_{14}$ and $Au_{65}Ga_{20.5}Eu_{14.5}$, were synthesized by arc-melting high-purity (>99.9 wt %) Au, Ga, and Eu raw elements. $Au_{66}Ga_{20}Eu_{14}$ was annealed at 873 K for 50 h under an Ar atmosphere, while $Au_{65}Ga_{20.5}Eu_{14.5}$ was first annealed at 1273 K for 5 h and then at 873 K for 1 week in order to improve the sample quality. The phase purity of the samples was examined by powder x-ray diffraction (XRD; Rigaku MiniFlex600) with Cu $K\alpha$ radiation, and also by scanning electron microscopy (SEM; JEOL JSM-IT100) together with energy-dispersive x-ray spectroscopy (EDX). Backscattered electron images for $Au_{66}Ga_{20}Eu_{14}$ and $Au_{65}Ga_{20.5}Eu_{14.5}$ are presented in the Supplemental Material [30], which shows that there is no trace of a second phase on a micrometer scale. In the powder XRD patterns for $Au_{66}Ga_{20}Eu_{14}$ and $Au_{65}Ga_{20.5}Eu_{14.5}$ shown in Fig. 2, all the peaks can be assigned to the 1/1 and 2/1 cubic approximants

*Corresponding author: tamura@rs.noda.tus.ac.jp

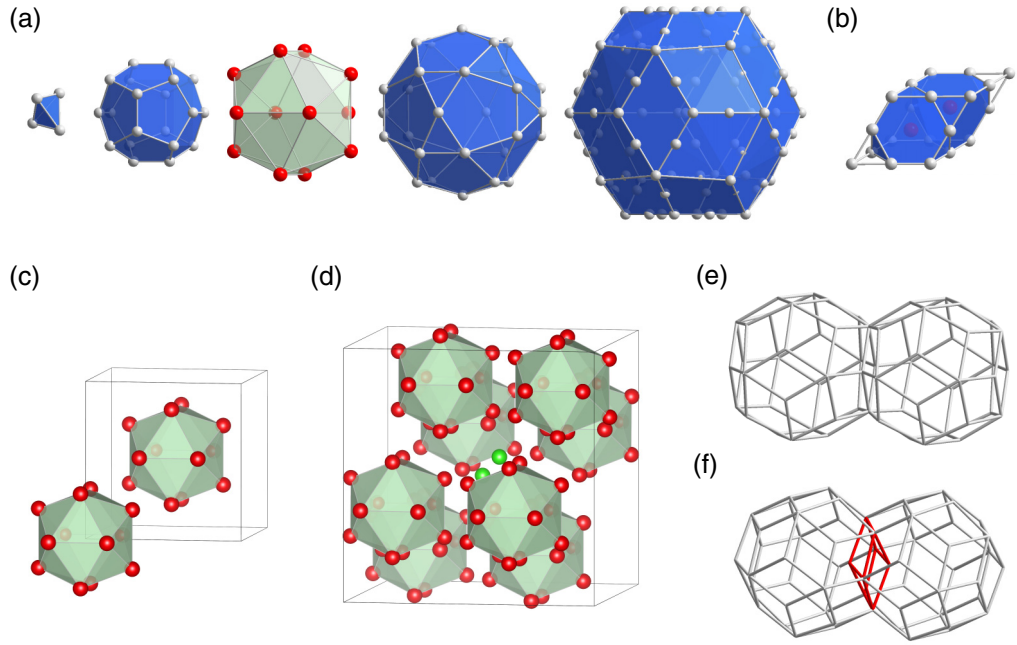

FIG. 1. Two building blocks of Tsai-type Cd-Yb 1/1 and 2/1 approximants: (a) Tsai-type rhombic triacontahedron (RTH) cluster and (b) acute rhombohedron (AR). White and red balls represent Cd and Yb, respectively. Atomic arrangements of Yb atoms in (c) 1/1 and (d) 2/1 approximants. Red and green balls represent Yb atoms located on the icosahedron shell and on the two sites inside the acute rhombohedron (AR), respectively. Two different RTH cluster connections: (e) *b* linkage and (f) *c* linkage.

with lattice parameters of 15.120 60(21) and 24.380 40(45) Å, respectively. The temperature and field dependence of the magnetization were measured using a magnetic property measurement system (MPMS; Quantum Design) in the temperature range between 2 and 300 K and at magnetic fields of up to 7 T. The temperature dependence of the magnetization was measured upon heating with a field of 10 mT after cooling to the lowest temperature with zero field [zero-field cooling (ZFC)] or with a field of 10 mT [field cooling (FC)]. The specific heat was measured using a physical property measurement system (PPMS; Quantum Design) by the relaxation method between 2 and 15 K, and under fields of 0 and 9 T.

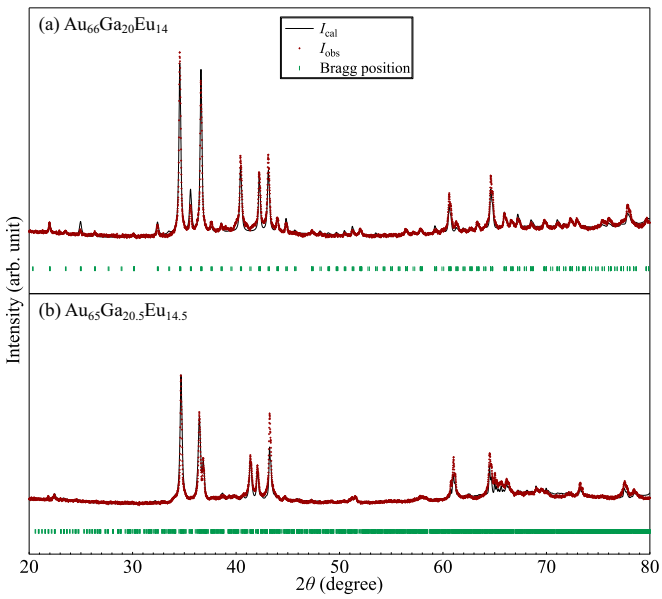

FIG. 2. Cu $K\alpha$ powder x-ray diffraction patterns for (a) $Au_{66}Ga_{20}Eu_{14}$ and (b) $Au_{65}Ga_{20.5}Eu_{14.5}$, together with the results of Le Bail fitting. I_{obs} (red dots) and I_{cal} (solid line) represent measured and calculated intensities, respectively. The positions of Bragg peaks are marked by green vertical bars. All peaks can be assigned to 1/1 and 2/1 cubic approximants with lattice parameters of 15.120 60(21) and 24.380 40(45) Å, respectively.

Figure 3 shows the temperature dependence of the inverse magnetic susceptibility $1/\chi$ for the 1/1 and 2/1 Au-Ga-Eu approximants in the temperature range of 2–300 K. The susceptibilities well obey the Curie-Weiss law,

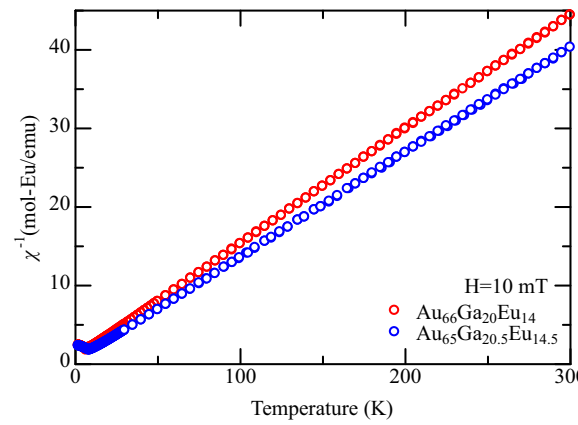

FIG. 3. Temperature dependence of inverse magnetic susceptibility χ^{-1} for 1/1 $Au_{66}Ga_{20}Eu_{14}$ and 2/1 $Au_{65}Ga_{20.5}Eu_{14.5}$.

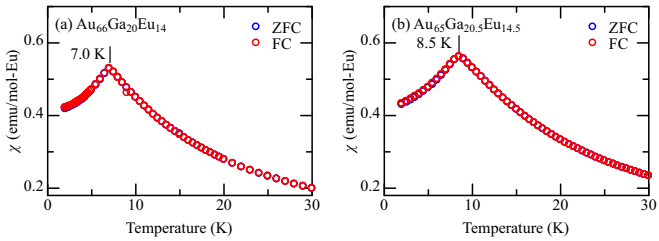

FIG. 4. Temperature dependences of ZFC and FC magnetic susceptibilities for (a) 1/1 $Au_{66}Ga_{20}Eu_{14}$ and (b) 2/1 $Au_{65}Ga_{20.5}Eu_{14.5}$ at low temperature (<30 K). Sharp cusps are observed at $T_N = 7.0$ and 8.5 K, respectively, evidencing AFM transitions at T_N.

$\chi = \frac{N_A \mu_{\rm eff}^2 \mu_B^2}{3k_B(T-\Theta_p)}$, for both approximants, as manifested by the excellent linearity in the $1/\chi$-T curves, where k_B, Θ_p, N_A, $\mu_{\rm eff}$, and μ_B are the Boltzmann constant, the paramagnetic Curie temperature, Avogadro's number, the effective moment, and the Bohr magneton, respectively. The results of least-squares fitting to the Curie-Weiss law between 50 and 300 K were $\mu_{\rm eff} = 7.400(8)\mu_B$, $\Theta_p = -4.458(18)$ K for 1/1 $Au_{66}Ga_{20}Eu_{14}$, and $\mu_{\rm eff} = 7.750(3)\mu_B$, $\Theta_p = -1.70(5)$ K for 2/1 $Au_{65}Ga_{20.5}Eu_{14.5}$. Both $\mu_{\rm eff}$ values are comparable to the theoretical value for free Eu^{2+} ions, 7.94 μ_B, which indicates that the Eu atoms are in the Eu^{2+} (isoelectronic to Gd^{3+}) state having a localized spin for both approximants. The slightly negative Θ_p values suggest that the net magnetic interaction acting on each spin is antiferromagnetic for both the 1/1 and 2/1 Au-Ga-Eu approximants.

Figures 4(a) and 4(b) show the temperature dependence of the ZFC and FC magnetic susceptibilities for 1/1 $Au_{66}Ga_{20}Eu_{14}$ and 2/1 $Au_{65}Ga_{20.5}Eu_{14.5}$, respectively. The occurrence of magnetic transitions is clearly evidenced by sharp cusps at $T_N = 7.0$ K and $T_N = 8.5$ K for 1/1 $Au_{66}Ga_{20}Eu_{14}$ and 2/1 $Au_{65}Ga_{20.5}Eu_{14.5}$, respectively. In addition, no appreciable difference is observed between the ZFC and FC curves for either approximant, suggesting the absence of nearly degenerate states near the ground state. The absence of frustration has already been inferred from a recent neutron diffraction experiment on the 1/1 AFM Au-Al-Tb approximant with a similar e/a value [31]. Figures 5(a) and 5(b) show the magnetic field dependence of the magnetization M for 1/1 $Au_{66}Ga_{20}Eu_{14}$ and 2/1 $Au_{65}Ga_{20.5}Eu_{14.5}$,

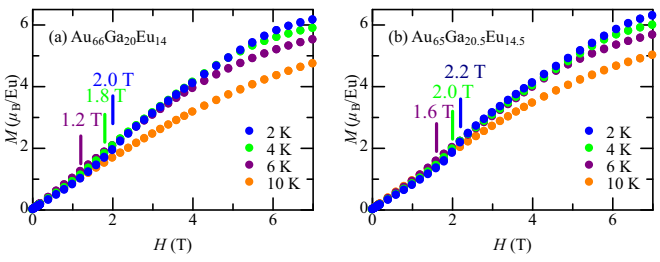

FIG. 5. Magnetization M of (a) 1/1 $Au_{66}Ga_{20}Eu_{14}$ and (b) 2/1 $Au_{65}Ga_{20.5}Eu_{14.5}$ as a function of magnetic field up to 7 T at 2, 4, 6, and 10 K. Spin flops are observed at the fields indicated by ticks. The spin-flop fields H_{SF} are determined from the dM/dH vs H maxima. H_{SF} increases with decreasing temperature, being consistent with the occurrence of an AFM transition for both compounds.

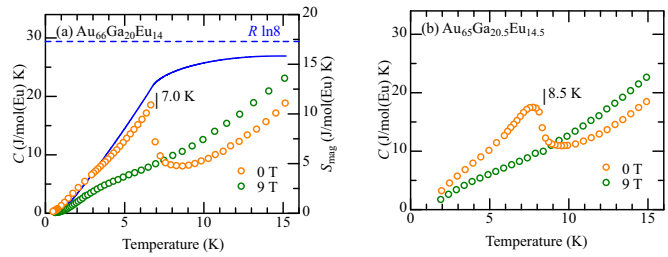

FIG. 6. Temperature dependences of the specific heat measured at 0 and 9 T for (a) 1/1 $Au_{66}Ga_{20}Eu_{14}$ and (b) 2/1 $Au_{65}Ga_{20.5}Eu_{14.5}$. A lambda anomaly due to the AFM transition is clearly observed for both compounds. The anomalies are suppressed in a field of 9 T, which is consistent with the occurrence of AFM transitions. In (a), the magnetic entropy is also shown, which is estimated by using the specific heat of the nonmagnetic 1/1 Au-Al-Y as a reference.

respectively, in fields of up to 7 T. Below T_N, the dM/dH vs H curves (not shown) exhibit a maximum at the magnetic fields denoted by the ticks, indicating that a metamagnetic anomaly exists for both the 1/1 and 2/1 approximants. Such a spin-flop phenomenon has also been observed in the case of 1/1 Au-Al-(Gd,Tb) AFM approximants [20]. The magnetic field corresponding to the spin flop H_{SF} is found to increase with decreasing temperature. Both the metamagnetic anomaly and the field dependence of H_{SF} corroborate the finding that the transitions are antiferromagnetic for both approximants. Figures 6(a) and 6(b) plot the temperature dependence of the specific heat C for the 1/1 and 2/1 Au-Ga-Eu approximants, respectively, measured at zero field and 9 T. A well-defined lambda anomaly is clearly observed at T_N for both compounds at zero field, which is also consistent with the AFM transition at T_N. These anomalies disappear under a magnetic field of 9 T, as shown in Figs. 6(a) and 6(b), which indicates the suppression of the AFM order at fields above H_{SF}. Here, a broad shoulder is noticed around 3 K in the C-T curve for both the Au-Ga-Eu approximants. A similar broad feature is also present for 1/1 Au-Si-Gd [15] and 1/1 Au-Al-Gd [20] but not for 1/1 Au-Al-Tb [20]. Since the Eu^{2+} ion is isoelectronic to the Gd^{3+} ion, it suggests that the observed broad features commonly seen in the Eu and Gd systems are of the same origin. Figure 6(a) also shows the magnetic entropy S_m of 1/1 Au-Ga-Eu, which is estimated by using the specific heat of the nonmagnetic 1/1 Au-Al-Y as a reference. It is seen that the magnetic entropy approaches $R \ln 8$ as the temperature approaches 15 K.

Figure 7 shows the magnetic phase diagram for the Tsai-type 1/1 approximant in terms of the e/a ratio, which was obtained from a recent detailed study on the 1/1 Au-Al-Gd approximant [20]. The figure clearly demonstrates that the ground state of Tsai-type 1/1 approximants is well classified by a *single* parameter, namely, the e/a ratio, and, in particular, it provides the condition for the occurrence of an AFM phase for Tsai-type 1/1 approximants, which is $1.54 < e/a < 1.56$. Such variation of Θ_p with the e/a ratio can be understood by considering that the net Ruderman-Kittel-Kasuya-Yosida (RKKY) interaction acting on each spin is dependent on the e/a ratio on the basis of the free-electron approximation [20]. The e/a values for both the 1/1 and 2/1 Au-Ga-Eu

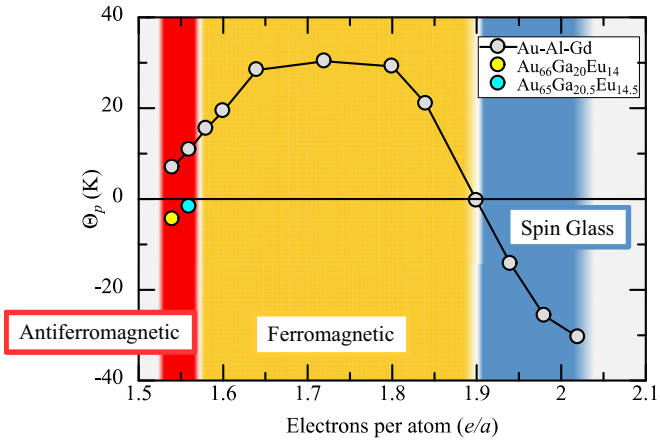

FIG. 7. Magnetic phase diagram for Tsai-type 1/1 approximant plotted in terms of the average electron-per-atom (e/a) ratio for the Au-Al-Gd approximant [20]. The magnetic orders observed at 2.2 K are shown. The paramagnetic Curie temperature Θ_p is also shown as a function of e/a. The AFM order is found within a narrow e/a window: $e/a = 1.54-1.56$. The e/a ratios for both the 1/1 and 2/1 Au-Ga-Eu AFM approximants are plotted together with their Θ_p values. Both e/a ratios are located within the narrow e/a window of the AFM phase.

approximants are plotted in the figure on the basis of the assumption that Au, Eu, and Ga are monovalent, divalent, and trivalent, respectively. Both the 1/1 and 2/1 Au-Ga-Eu AFM phases are found to be located within the above-mentioned e/a region of 1.54–1.56, validating the magnetic phase diagram, even for the 2/1 approximant. We note that the Θ_p values are small for the Au-Ga-Eu AFM approximants, which indicates that FM and AFM interactions coexist as in the case of the 1/1 Au-Al-Gd approximant.

Very recently, Sato *et al.* [31] reported that the AFM order for the 1/1 Au-Al-Tb approximant can be explained by the coexistence of FM and AFM interactions, i.e., AFM interactions between the nearest-neighbor spins ($J_1 < 0$) and FM interactions between the second-nearest-neighbor spins ($J_2 > 0$) where the magnetic interaction E is defined as $E = -\sum_{ij} J_{ij} \vec{R}_i \cdot \vec{R}_j$, with $\vec{R}_i$ and $\vec{R}_j$ the positions of the ith and jth spins, respectively. This coexistence of FM and AFM interactions accounts for the small Θ_p value observed for the Au-Al-Tb approximant. Moreover, they reported that the 1/1 Au-Al-Tb AFM phase has no frustration, i.e., the ground state is uniquely determined for the obtained set of J_1 and J_2 values. Since the e/a values for the present Au-Ga-Eu AFM approximants are almost the same as that for the 1/1 Au-Al-Tb AFM approximant, the small Θ_p values for the Au-Ga-Eu AFM approximants can also be understood as the result of the opposite signs of J_1 and J_2. The absence of spin freezing in the Au-Ga-Eu approximants is also attributed to the absence of frustration. One significant finding of the present work is that the AFM order in the 1/1 approximant survives when the degree of approximation to a quasicrystal is increased, provided that the e/a ratio is kept nearly the same. Although the 2/1 approximant contains two additional R atoms inside an AR that is absent in 1/1 approximants, the Néel temperatures and both the $\chi-T$ and M-H curves are found to be comparable for the two types of approximants, suggesting that the role of the additional Eu^{2+} spins in the magnetism is limited. Thus, both of the above results suggest that AFM quasicrystals may exist for comparable e/a values, likely within the 1.54–1.56 range, and further work is now under progress.

In conclusion, we have reported AFM transitions in both 1/1 and 2/1 Au-Ga-Eu quasicrystal approximants having comparable e/a ratios. Both the magnetic susceptibility and the specific heat show that the 1/1 and 2/1 approximants undergo an AFM transition at $T_N = 7.0$ and 8.5 K, respectively. The AFM orders in the 1/1 and 2/1 Au-Ga-Eu approximants are observed for e/a ratios that are consistent with the AFM region obtained for the 1/1 Au-Al-Gd approximant, suggesting that the e/a ratio is the key controlling parameter for the magnetism, also for higher-order Tsai-type quasicrystal approximants. Since the 2/1 approximant has all the building blocks necessary for the corresponding quasicrystal, the present discovery of the 2/1 AFM approximant may pave the way for the realization of long-sought AFM quasicrystals through tuning of the e/a ratio; work to this end is currently underway.

This work was supported by a Kakenhi Grant-in-Aid (No. 19H05818) from the Japan Society for the Promotion of Science (JSPS).

S.Y. and S.S. contributed equally to the work.

[1] A. P. Tsai, J. Q. Guo, E. Abe, H. Takakura, and T. J. Sato, Nature (London) **408**, 537 (2000).
[2] J. Q. Guo, E. Abe, and A. P. Tsai, Phys. Rev. B **62**, R14605 (2000).
[3] C. P. Gómez and S. Lidin, Phys. Rev. B **68**, 024203 (2003).
[4] A. P. Tsai, Chem. Soc. Rev. **42**, 5352 (2013).
[5] R. Tamura, Y. Murao, S. Takeuchi, M. Ichihara, M. Isobe, and Y. Ueda, Jpn. J. Appl. Phys. **41**, L524 (2002).
[6] T. Ishimasa, Y. Kasano, A. Tachibana, S. Kashimoto, and K. Osaka, Philos. Mag. **87**, 2887 (2007).
[7] T. Yamada, R. Tamura, Y. Muro, K. Motoya, M. Isobe, and Y. Ueda, Phys. Rev. B **82**, 134121 (2010).
[8] K. Nishimoto, T. Sato, and R. Tamura, J. Phys.: Condens. Matter **25**, 235403 (2013).
[9] R. Tamura, J. Phys.: Condens. Matter **27**, 085401 (2015).
[10] R. Tamura, Y. Muro, T. Hiroto, K. Nishimoto, and T. Takabatake, Phys. Rev. B **82**, 220201(R) (2010).
[11] M. G. Kim, G. Beutier, A. Kreyssig, T. Hiroto, T. Yamada, J. W. Kim, M. de Boissieu, R. Tamura, and A. I. Goldman, Phys. Rev. B **85**, 134442 (2012).

[12] R. Tamura, Y. Muro, T. Hiroto, H. Yaguchi, G. Beutier, and T. Takabatake, Phys. Rev. B **85**, 014203 (2012).
[13] A. Mori, H. Ota, S. Yoshiuchi, K. Iwakawa, Y. Taga, Y. Hirose, T. Takeuchi, E. Yamamoto, Y. Haga, F. Honda, R. Settai, and Y. Ōnuki, J. Phys. Soc. Jpn. **81**, 024720 (2012).
[14] A. Kreyssig, G. Beutier, T. Hiroto, M. G. Kim, G. S. Tucker, M. de Boissieu, R. Tamura, and A. I. Goldman, Philos. Mag. Lett. **93**, 512 (2013).
[15] T. Hiroto, G. H. Gebresenbut, C. P. Gómez, Y. Muro, M. Isobe, Y. Ueda, K. Tokiwa, and R. Tamura, J. Phys.: Condens. Matter **25**, 426004 (2013).
[16] T. Hiroto, K. Tokiwa, and R. Tamura, J. Phys.: Condens. Matter **26**, 216004 (2014).
[17] G. H. Gebresenbut, M. S. Andersson, P. Beran, P. Manuel, P. Nordblad, M. Sahlberg, and C. P. Gómez, J. Phys.: Condens. Matter **26**, 322202 (2014).
[18] G. H. Gebresenbut, M. S. Andersson, P. Nordblad, M. Sahlberg, and C. P. Gómez, Inorg. Chem. **55**, 2001 (2016).
[19] A. Ishikawa, T. Hiroto, K. Tokiwa, T. Fujii, and R. Tamura, Phys. Rev. B **93**, 024416 (2016).
[20] A. Ishikawa, T. Fujii, T. Takeuchi, T. Yamada, Y. Matsushita, and R. Tamura, Phys. Rev. B **98**, 220403(R) (2018).
[21] D. Kawana, T. Watanuki, A. Machida, T. Shobu, K. Aoki, and A. P. Tsai, Phys. Rev. B **81**, 220202(R) (2010).
[22] T. Watanuki, S. Kashimoto, D. Kawana, T. Yamazaki, A. Machida, Y. Tanaka, and T. J. Sato, Phys. Rev. B **86**, 094201 (2012).
[23] K. Deguchi, S. Matsukawa, N. K. Sato, T. Hattori, K. Ishida, H. Takakura, and T. Ishimasa, Nat. Mater. **11**, 1013 (2012).
[24] K. Deguchi, M. Nakayama, S. Matsukawa, K. Imura, K. Tanaka, T. Ishimasa, and N. K. Sato, J. Phys. Soc. Jpn. **84**, 023705 (2015).
[25] K. Deguchi, M. Nakayama, S. Matsukawa, K. Imura, K. Tanaka, T. Ishimasa, and N. K. Sato, J. Phys. Soc. Jpn. **84**, 015002 (2015).
[26] K. Kamiya, T. Takeuchi, N. Kabeya, N. Wada, T. Ishimasa, A. Ochiai, K. Deguchi, K. Imura, and N. K. Sato, Nat. Commun. **9**, 154 (2018).
[27] C. P. Gómez and S. Lidin, Angew. Chem., Int. Ed. **40**, 4037 (2001).
[28] H. Takakura, C. P. Gómez, A. Yamamoto, M. de Boissieu, and A. P. Tsai, Nat. Mater. **6**58, (2007).
[29] D. Shechtman, I. Blech, D. Gratias, and J. W. Cahn, Phys. Rev. Lett. **53**, 1951 (1984).
[30] See Supplemental Material at http://link.aps.org/supplemental/10.1103/PhysRevB.100.180409 for backscattered electron images for the $Au_{66}Ga_{20}Eu_{14}$ and $Au_{65}Ga_{20.5}Eu_{14.5}$ compounds.
[31] T. J. Sato, A. Ishikawa, A. Sakurai, M. Hattori, M. Avdeev, and R. Tamura, Phys. Rev. B **100**, 054417 (2019).